Journal of Innovative Optical Health Sciences
Vol. 7, No. 5 (2014) 1450027 (10 pages)

DOI: 10.1142/S1793545814500278

World Scientific
www.worldscientific.com

Multimodal nonlinear imaging of atherosclerotic plaques differentiation of triglyceride and cholesterol deposits

Christian Matthäus[*,†], Riccardo Cicchi[‡,§], Tobias Meyer[*], Annika Lattermann[¶], Michael Schmitt[†], Bernd F. M. Romeike[‖], Christoph Krafft[*], Benjamin Dietzek[*,†], Bernhard R. Brehm[**], Francesco S. Pavone[§] and Jürgen Popp[*,†,††]

[*]*Leibniz Institute of Photonic Technology (IPHT-Jena)*
Albert Einstein Straße 9, 07745 Jena, Germany

[†]*Institute of Physical Chemistry and Abbe Center of Photonics*
Friedrich Schiller University Jena, Helmholtzweg 4, 07743 Jena, Germany

[‡]*National Institute of Optics, National Research Council (INO-CNR)*
Largo E. Fermi 6 – 50125, Florence, Italy

[§]*European Laboratory for Non-Linear Spectroscopy (LENS)*
University of Florence Via Nello Carrara
1-50019, Sesto Fiorentino (Firenze), Italy

[¶]*Clinic for Internal Medicine, Jena University Hospital*
Friedrich-Schiller-University, Erlanger Allee 101, 07747 Jena, Germany

[‖]*Institute of Pathology, Department of Neuropathology*
Jena University Hospital – Friedrich-Schiller-University
Erlanger Allee 101, 07740 Jena, Germany

[**]*Catholic Clinic — Koblenz, Internal Medicine & Cardiology*
Rudolf Virchow Str. 9, 56073 Koblenz, Germany
[††]*juergen.popp@ipht-jena.de*

Received 16 October 2013
Accepted 26 December 2013
Published 24 February 2014

Cardiovascular diseases in general and atherothrombosis as the most common of its individual disease entities is the leading cause of death in the developed countries. Therefore, visualization and characterization of inner arterial plaque composition is of vital diagnostic interest, especially

for the early recognition of vulnerable plaques. Established clinical techniques provide valuable morphological information but cannot deliver information about the chemical composition of individual plaques. Therefore, spectroscopic imaging techniques have recently drawn considerable attention. Based on the spectroscopic properties of the individual plaque components, as for instance different types of lipids, the composition of atherosclerotic plaques can be analyzed qualitatively as well as quantitatively. Here, we compare the feasibility of multimodal nonlinear imaging combining two-photon fluorescence (TPF), coherent anti-Stokes Raman scattering (CARS) and second-harmonic generation (SHG) microscopy to contrast composition and morphology of lipid deposits against the surrounding matrix of connective tissue with diffraction limited spatial resolution. In this contribution, the spatial distribution of major constituents of the arterial wall and atherosclerotic plaques like elastin, collagen, triglycerides and cholesterol can be simultaneously visualized by a combination of nonlinear imaging methods, providing a powerful label-free complement to standard histopathological methods with great potential for *in vivo* application.

Keywords: Nonlinear microscopy; Raman spectroscopy; atherosclerosis.

1. Introduction

Atherosclerosis is the leading cause of death in western countries.[1] Due to risk factors, such as fatty diets, smoking, aging and oxidative stress, endothelial cells become susceptible to permeation and deposition of various lipids circulating through the bloodstream, as well as crystalline calcium.[2] This process initiates a chronic inflammation of the vessel wall and is followed by a migration of monocytes, a type of white blood cells that differentiate into macrophages, which are responsible for lipid incorporation within tissues. If these cells are overwhelmed with the metabolic stress, the subsequent cell death and cellular debris contributes to the arterial swelling.[3] Continuous swelling can lead to the rupture of these plaque deposits, with often fatal consequences such as heart attack or stroke.[3,4] The composition of inner arterial plaques can vary with the influence of various risk factors, as for instance hypertension, hyperlipidemia, insulin resistance, smoking or adipositas. Furthermore, different types of medication also have an influence on makeup and evolution of these deposits.

Conventional histopathological protocols, such as staining with hematoxylin/eosin (H&E), Verhoeff-Van Gieson or Oil-Red, are used to contrast such plaque deposits against connective tissue and to some extent are able to distinguish the most common plaque components, such as cholesterol or crystalline calcium. For *in vivo* noninvasive diagnosis, contrasting tools commonly used in medical imaging as for instance magnetic resonance imaging (MRI) or X-ray angiography are available. For invasive diagnosis, catheter-based techniques such as intravascular ultrasound (IVUS) and optical coherence tomography (OCT) probes are already established for clinical application.[5] All of these techniques provide black and white contrast but are very limited with respect to both spatial resolution and biochemical information.[6] In order to obtain qualitative and quantitative insight, several spectroscopic techniques have been suggested, which may be coupled to microscopes for comparison with standard histopathology or endoscopes for application *in vivo*. Because of high sensitivity and label-free imaging capability nonlinear micro-spectroscopic techniques are very promising. Collagen can be easily imaged by second-harmonic generation (SHG) microscopy due to its noncentrosymmetric molecular structure, which is rare for biological molecules. Lipids, which strongly contribute to plaque deposits, have a very high scattering cross section and give rise to very strong coherent anti-Stokes Raman scattering (CARS) signals.[7–9] Autofluorescence can also deliver additional information about the composition of plaques and provide a label-free contrast method for elastic fibers in the arterial walls. Various experiments on this topic have already been reported so far. Lipid accumulating macrophages have been observed by CARS microscopy on porcine aorta and hyperlipidemic rabbit aorta thin sections in combination with SHG and two-photon fluorescence (TPF).[10–14] Crystalline cholesterol, which can be built up over time in the intra- as well as extra-cellular space and may potentially injure surrounding connective tissue,

can be visualized by either CARS or stimulated Raman scattering (SRS), which was demonstrated also in combination with SHG.[14–16] For endoscopic *in vivo* applications, Raman spectroscopy also in combination with fluorescence and diffuse reflectance spectroscopy have been suggested.[17,18] Since the likeliness of severe cardiovascular disease depends critically on the composition of the plaque deposition, imaging techniques offering molecular contrast are required. In this contribution, we confirm that major constituents of the arterial wall and atherosclerotic plaques can be simultaneously visualized and characterized by a combination of nonlinear imaging methods. In addition, we provide evidence that the CARS effect gives rise to signals from all lipid components of the plaque formation, whereas SHG reveals cholesterol and cholesterolesters, by using Raman microscopy.

2. Materials and Methods

2.1. *Rabbit model*

Animals: In combination with other investigations, 17 adult male *New Zealand White* rabbits (Harlan, Borchen, Germany) were studied. To generate atherosclerotic changes of the vascular system, rabbits were fed with a 0.5% cholesterol diet for different periods (7–10 weeks). For the nonlinear imaging experiments, different positions of six aortas were investigated.

Animal Sacrifice/Pressure Perfusion/ Sample Preparation: The rabbits were sacrificed by an overdose of the anesthetic solution of ketamine and xylazine. With a vertical thoracic to abdominal incision, the aorta was prepared and a perfusion cannula was inserted into the descending aorta. A 150 mL mixture of 10% hydroxyethyl starch (Fresenius Kabi Deutschland GmbH, Bad Homburg, Germany) and 1% procain in ratio of 10:1 was used for vessel fixation, followed by a 0.9% saline (Fresenius Kabi Deutschland GmbH, Bad Homburg, Germany) pressure perfusion over 15 min at 100 mmHg. The complete aorta was excised and preserved in 5% formalin solution (Oscar Fischer GmbH, Saarbrücken, Germany) for further *ex vivo* nonlinear imaging acquisitions. Thin (5 μm thick) tissue cross sections were prepared using a microtome without standard embedding material to avoid strong signal contributions from the commonly used polymeric embedding matrix. The aortas were fixed in formalin, to prevent the sample from degradation after the extraction. Formalin cross-links the proteins of the sample and has among the established fixation techniques the least effect on lipids.

Tissue cross sections were placed on CaF_2 slides to avoid strong fluorescence from regular glass during the Raman measurements. For multimodal imaging of the inner arterial wall, the blood vessel was cut along the direction of the blood flow. In order to have the inner arterial wall exposed, for the inverse microscopic setup, the tissue was sandwiched in a small chamber between two microscope cover slips. The sample was immersed in a physiological buffer during the measurement in order to prevent denaturation and shrinkage due to drying.

2.2. *CARS and TPF microscopic imaging*

The employed setup for CARS microscopy has been described in detail elsewhere.[19] Briefly, the laser source consists of a Ti:Sapphire laser (Mira HP from Coherent) pumped by a Nd:Vanadate laser (Verdi-V18 from Coherent) at 532 nm. The Ti:Sa oscillator generates 2 ps-pulses at a wavelength of 830 nm (full with at half maximum (FWHM) $\sim$ 1.5 nm), a repetition rate of 76 MHz and an average power of approximately 3 W. A 60:40 beam splitter divides the laser beam into two parts: one part is used as Stokes and is further attenuated; the other one pumps an optical parametric oscillator (APE Berlin, Germany) to provide the pump pulse at 669.5 nm with a FWHM of about 0.7 nm and a typical output power of 150–200 mW for the two-color CARS scheme.[20] A delay stage, a retro-reflector and a dichroic mirror (LP 800, Omega optics 3rd mill, USA) are used to recombine pump and Stokes laser temporally and spatially. The two beams are sent into a laser scanning microscope (LSM 510 Meta, Zeiss, Germany). The laser radiation is focused by an objective (Epi-plan neofluar, Zeiss, Germany) with 20-fold magnification and a NA of 0.5 onto the object plane. The anti-Stokes signal at 561 nm depends on the sample detected in either forward (aorta cross sections) or in Epi-direction (z-stacks of aorta vessel wall) by a photomultiplier tube (Hamamatsu R6357) after separating the excitation beams through short-pass filters (Omega Optical, 3rd millennium, USA). CARS, TPF and SHG images of aorta cross sections were recorded first in mosaic modus in order to scan a large area of multiple

images. Each CARS image had a field of view of 450 $\times 450\,\mu m^2$ and a resolution of 1024×1024 pixels. At locations of interest, further images were acquired. For *in vitro* imaging of whole arterial walls immersed in buffer, depth profiles (z-stacks) were measured, recording 15 optically sectioned images separated by 5 μm each. The pixel dwell time was 1.6 μs resulting in an acquisition time per image plane of 3 to 4 min including an 8-fold averaging. The power at the objective pupil of both lasers was 60 mW.

TPF imaging was performed simultaneously to the acquisition of CARS microscopic images illuminating the sample with both Stokes and pump beams (830.7 and 669.5 nm, respectively) enabling two photon excitation of tissue endogenous fluorophores absorbing in the blue-UV range of the spectrum, e.g., NADH and elastin. The TPF signal was detected in the backward direction using a descanned photomultiplier in the scan module. For removal of the excitation laser, two short-pass filters with cutoff at 615 and 545 nm were used and the fluorescence emission was detected in the 435–485 nm range using a bandpass filter.

2.3. *SHG microscopic imaging*

For SHG imaging, only the laser at 830 nm was used and the signal was detected in both forward and backward directions by non-descanned photomultiplier tube (PMT) modules. For filtering a combination, a short-pass filter at 610 nm and a narrow bandpass filter at 415 nm with a FWHM of 3 nm (Omega Optical, USA) were employed in both channels. SHG images were obtained by summing the signals detected in the two channels. For thick tissue specimens, only backward detection was used. For post-processing of the CARS, TPF and SHG images ImageJ (National Institutes of Health, Bethesda, MD, USA) was employed.

2.4. *Raman imaging*

Raman images were acquired using a Confocal Raman Microscope Model CRM alpha300R (WITec, Ulm, Germany). Excitation at 785 nm (about 10 mW at the sample) is provided by a diode laser (Toptica Photonics AG, Gräfelfing, Germany). The exciting laser radiation is coupled into a Zeiss microscope through a wavelength-specific single mode optical fiber. The incident laser beam is collimated via an achromatic lens and passes a holographic bandpass filter before it is focused onto the sample through the objective of the microscope. A Zeiss EC Epiplan air objective ($50 \times /0.95$ NA) was used in the studies reported here. The sample is located on a piezo-electrically driven microscope scanning stage with a radial resolution of about 3 nm (± 5 nm repeatability), and an axial resolution of about 0.3 nm (± 2 nm repeatability). The sample is scanned through the laser focus in a raster pattern at a constant stage speed. The continuous motion prevents sample degradation in the focal point of the laser beam due to over exposure. Spectra were collected at a 1 μm grid with a dwell time of 0.25 s. Raman images were generated using a spectral unmixing algorithm based on vertex component analysis, which has been previously introduced for data analysis of biological samples.[21,22] Calculations were carried out using the MatLab software (MathWorks Inc., Natick, MA, USA).

3. Results

An H&E stained histopathology image of an arterial cross section with severe plaque formation is shown in Fig. 1(a). Clearly visible are deposits along the lumen of the aorta. Figure 1(b) shows a CARS image of an adjacent section recorded in resonance with the CH stretching modes of methylene groups especially abundant in lipids at 2850 cm^{-1}. Apparently, all lipid deposits within the lumen result in a strong CARS signal, whereas the connective tissue of the media generates a significantly lower signal which is not visible on this intensity scale. Thus, CARS at 2850 cm^{-1} selectively highlights plaque formations. Figure 1(c) shows a TPF image of the same section acquired simultaneously. Various biological molecules give rise to a strong fluorescence signal, which in the range of 670 to 830 nm may also be excited by means of two-photon excitation. In connective tissues, explicitly elastin gets excited with two photons, because of absorption properties in the blue range of the spectrum. Distinctly noticeable are the fibrous organization of the connective tissue in the media as well as the loose tissue of the lumen. In contrast to the CARS signals, TPF images both the protein structures of the membranes of the arterial wall and the plaques, since elastin in the protein fibers and oxidized lipoproteins in the plaque deposits give rise to fluorescence. Figure 1(d) shows the SHG signal collected from the

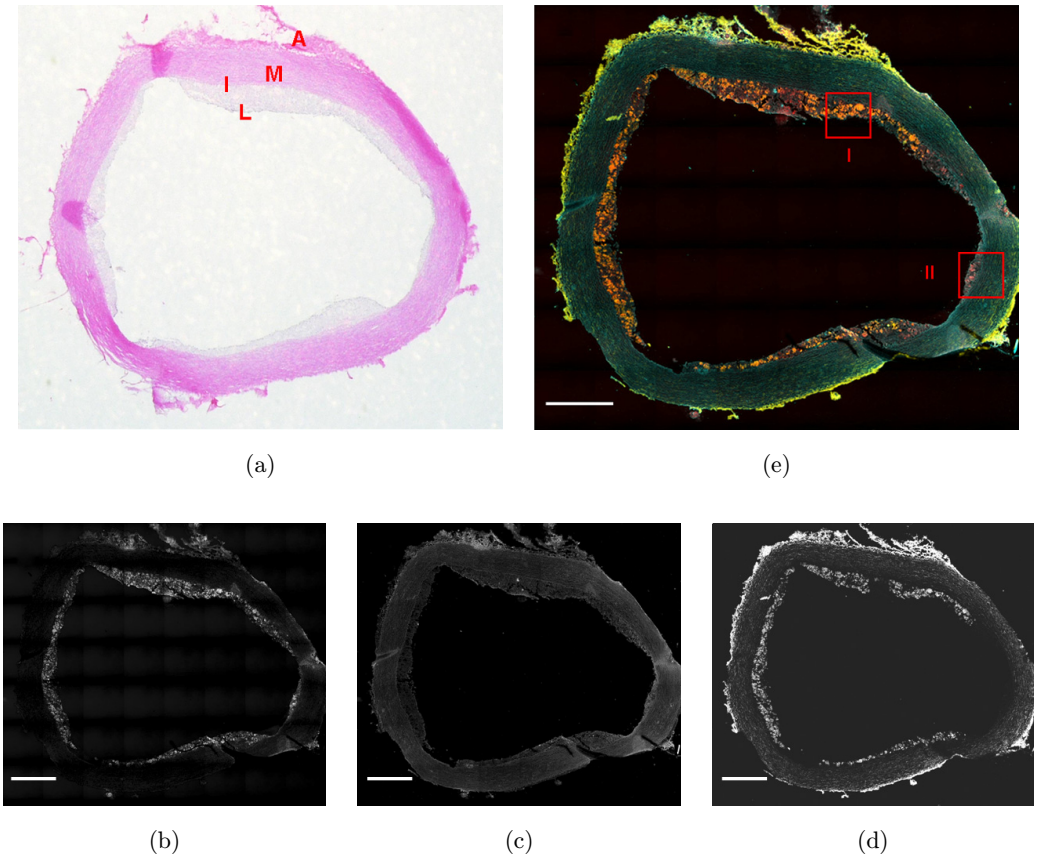

(a) (e)

(b) (c) (d)

Fig. 1. H&E stained histopathological image of a cross section of a rabbit aorta (a) in comparison with CARS (b), TPF (c) and SHG (d) images acquired from an adjacent section. Clearly noticeable are severe plaque deposits along the intima (I) and the lumen (L). Also visible are the media (M) and adventitia (A). The image shown in (e) is an overlay of the CARS (red), TPF (cyan) and SHG (yellow) signals. The scale bars are 0.5 mm.

same section. Interestingly, most of the structures provide a strong SHG signal. Because of the symmetry properties of collagen, again the connective tissue of the media and the adventitia are visible. Surprisingly, most intense signals are also observed from the lipid deposits. By comparing the SHG with the CARS image it is evident that there is a strong overlap between both signals, of about 80%, within the plaque areas. However, especially the plaque regions on the right part of the cross section show no SHG signal at all. Figure 1(e) is an overlay of the three channels, showing the CARS signal in red, the TPF signal in cyan and the SHG signal in yellow. The overlapping regions of the CARS and the SHG signals appear now in orange.

To obtain further information about the plaque composition and to assess the chemical origin of the differences revealed by CARS and SHG images, Raman images were acquired within regions where both signals were detected and where only CARS was observed. In Fig. 1(e), the regions are indicated as (I) and (II), respectively. An enlarged area of (I) and (II) can be seen in Figs. 2(a) and 2(b), respectively. The corresponding Raman images are shown in Figs. 2(c) and 2(d) along with the associated spectral information plotted in the graphs 2(e) and 2(f). The Raman images were reconstructed using a spectral decomposition algorithm that searches for the most dissimilar spectral information within the dataset. The abundances of the spectral information are plotted in corresponding false colors scale. Based on the spectral information, the main plaque component within region (I) can be clearly assigned to cholesterol and cholesterol ester, whereas the overwhelming plaque component in (II) can be assigned to triglycerides. Spectra (a) and (b), corresponding to the green and yellow regions in the Raman image, exhibit all the

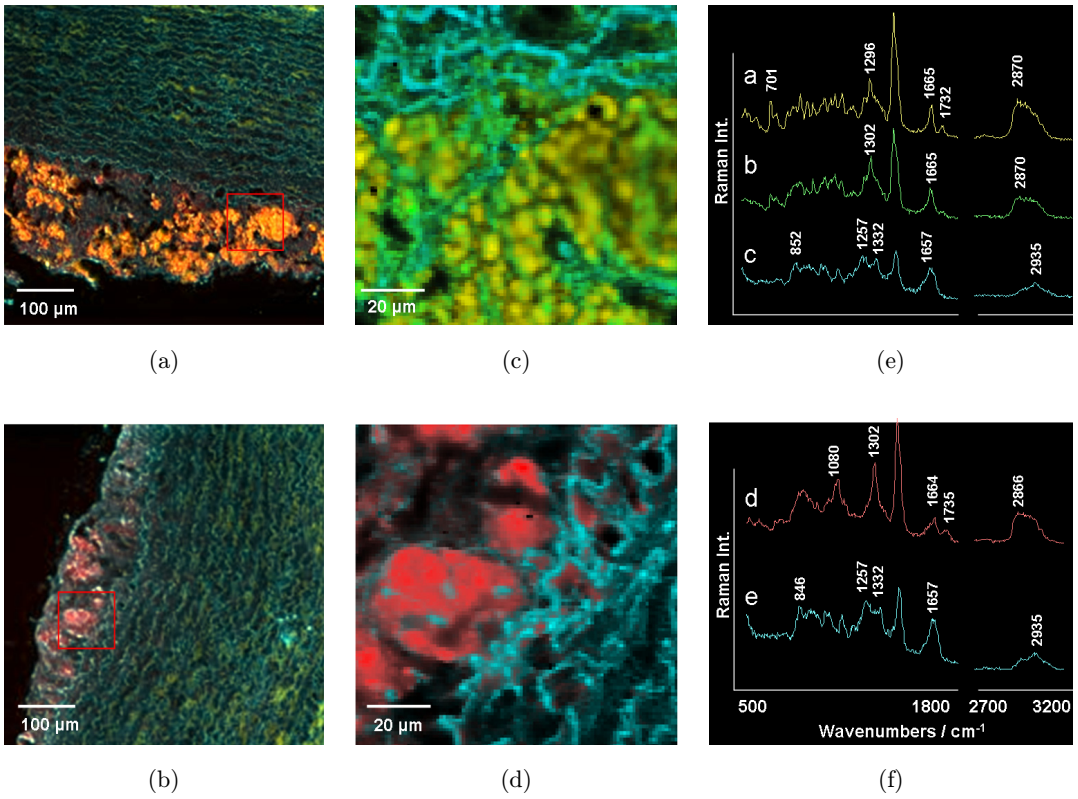

Fig. 2. Multimodal images of CARS (red), TPF (cyan) and SHG (yellow) signals of the two areas marked (I) and (II) in Fig. 1 and Raman images (c) and (d) of the indicated areas along with the associated spectral information plotted in (e) and (f). Within the Raman images, the spectra and the associated distribution of cholesterol esters are shown in yellow (a), cholesterol in green (b) and triglycerides in red (d). The surrounding connective tissue is plotted in cyan [(c) and (e)].

spectral features of cholesterol, as for instance the CH stretching between 2800 and 3100 cm^{-1}, the C=C stretching of the double bond at 1650 cm^{-1} or the deformations of the steran skeleton, very rich in Raman bands within the lower wavenumber region. Cholesterol esters can be distinguished spectroscopically by the C=O stretching of the ester linkage at 1745 cm^{-1}. The distribution of cholesterol and cholesterol esters are shown in green and yellow, respectively. Spectrum (d) shows all characteristic features of triglycerides. Both spectra have overlapping band positions; however, the spectral contrast is obvious. The spectra (c) and (e) mainly consist of protein bands and the distribution, plotted in cyan depicts the fine structure of the surrounding connective tissue. More detailed spectral assignments can be found in the literature.[23–25]

For potential endoscopic *in vivo* applications, visualization of the arterial wall perpendicular to the blood flow may be of interest, to address the issues of penetration depth and different focal planes of CARS, TPF and SHG. In order to investigate this top viewing approach, the section adjacent to the above-described cross section was prepared as described in Sec. 2. Figure 3 shows an example of CARS (a), TPF (b) and SHG (c) images of that section and an overlay (d), recorded under the same conditions as images of the cross section. The field of view is $450 \times 450\,\mu m^2$. A z-stack of images was obtained by scanning in 5 μm step size, 100 μm into the tissue, starting from the top. The images were constructed using a maximum intensity projection in the direction of the z-axis. The z-profile of the images is projected along the axes of the individual images in Fig. 3. Again, the CARS and SHG images reveal plaque deposits, whereas the TPF signal shows the connective tissue of the vessel wall visualized by SHG/TPF. The CARS and SHG images are super-imposable to a great extent, but are not identical. In addition to the structures revealed by SHG, the CARS image shows smaller more spherical plaque deposits. Considering the above-described Raman assignment, it is reasonable

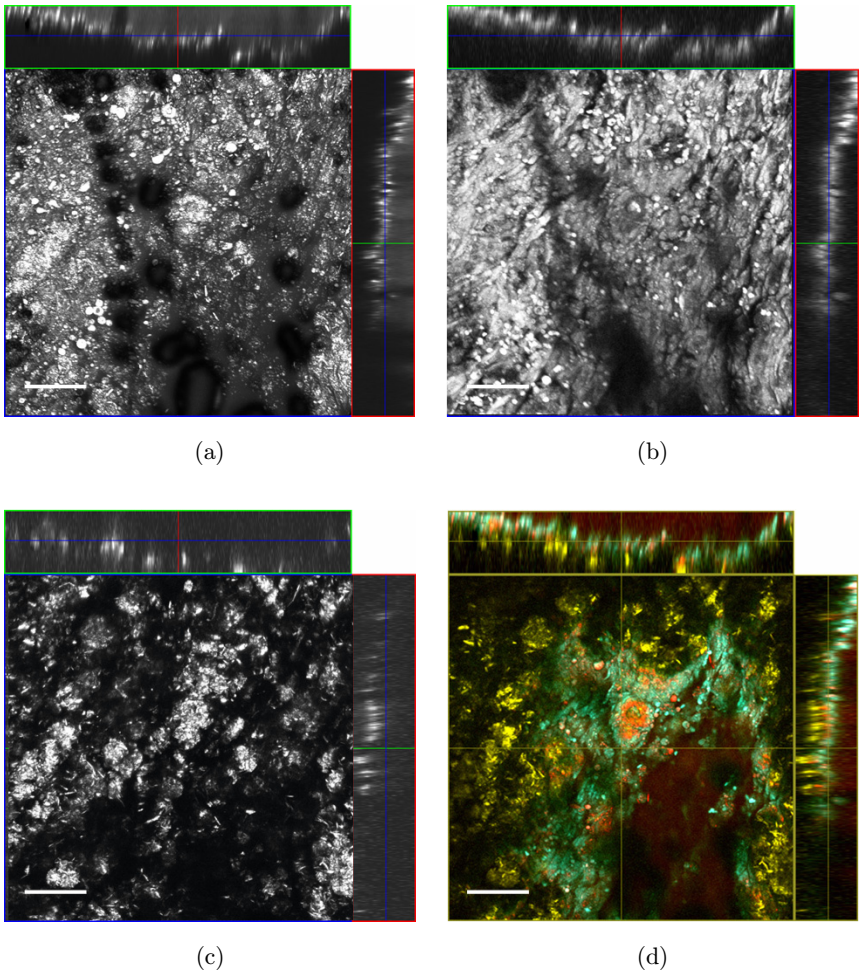

Fig. 3. CARS (a), TPF (b) and SHG (c) images of a plaque recorded as a z-stack of about 100 μm into the tissue at a step size of 5 μm. Image (d) is an overlay of all three signals, whereby the CARS signal is plotted in red, the TPF signal in cyan and the SHG signal in yellow. The field of view is $450 \times 450\,\mu\text{m}^2$. The scale bars are 100 μm. Image intensity and contrast of the three images in (a), (b) and (c) were properly adjusted before merging them in the overlaid image (d).

to assume that these are deposits mainly composed of triglycerides. In the overlaid image the CARS, TPF and SHG images are depicted in red, cyan and yellow, respectively. Areas with CARS and SHG signal contribution appear in pink. The image also shows small CARS and TPF overlapping signals, which appear in yellow. Here, the distribution of the connective tissue and the fatty deposits are not completely resolved.

The possibility to selectively image cholesterol deposition in the arterial wall using SHG microscopy was demonstrated using multimodal nonlinear imaging and confirmed by Raman spectral assignment. Additional examination performed on a thick tissue sample, imaged with the optical axis perpendicular to the blood flow provided additional support to this hypothesis. In Fig. 4(a), a multimodal nonlinear image combining CARS (red), TPF (cyan) and SHG (yellow) acquired at a depth of about 40 μm from sample surface is shown. The field of view is $450 \times 450\,\mu\text{m}^2$. As observed in Fig. 3, CARS and SHG images reveal plaque deposits, whereas TPF shows the connective tissue of the arterial wall. A small pink-colored rod is clearly distinguishable in the center of the image. A more detailed view of this particular structure is depicted in Fig. 4(b), where the small red square in Fig. 4(a) is reported on a magnified scale. This particular structure was found to provide strong CARS and SHG signals, as demonstrated by the Figs. 4(c) and 4(d), where the CARS and the SHG images are separately shown. This formation is thought to be a cholesterol crystal deposited within the arterial wall. The CARS signal is due to the CH

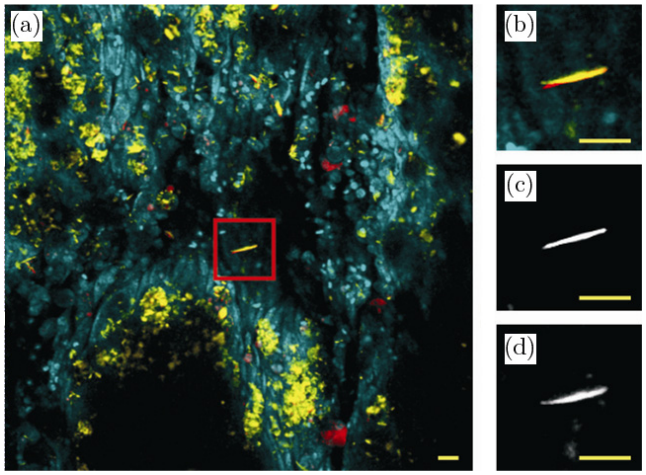

Fig. 4. CARS (red), TPF (cyan) and SHG (yellow) composed color image (a) recorded with *en face* optical geometry at a depth of about 40 μm from tissue surface. The particular image within the red square is shown on a magnified scale in (b). Cholesterol crystal within atherosclerotic plaque deposition (b). Image of the CARS signal (c) and SHG signal (d) of the image shown in B. Scale bars are 20 μm. Image intensity and contrast of the three images composing Fig. (a) was properly adjusted before merging them in the overlaid image (a) in order to highlight the fact that the cholesterol crystal located in the inset is emitting both CARS and SHG.

stretching vibrations, while the strong SHG signal observed is probably due to the nonlinear optical properties of cholesterol as well as to the regular molecular arrangement in a crystalline structure.

4. Discussion

CARS, TPF and SHG images were obtained from thin cross sections, as well as from bulk plaque formations at the inner arterial wall. Whereas the CARS signal, recorded in resonance with the maximum of the CH stretching vibrations of methylene groups predominant in lipids detected plaque deposits mainly composed of cholesterol, cholesterol ester and/or triglycerides, TPF revealed protein structures composed of elastin and oxidized lipids within the plaques. The results are in good agreement with earlier studies. Interestingly, SHG signals were generated from connective tissue as well as from plaque areas. It is well established that collagen, because of the symmetry of the triple helical arrangement of its protein strands, gives rise to strong SHG signals. Recently, it has been reported that crystalline cholesterol and cholesterol esters without crystalline structure can generate frequency doubling.[15] The Raman images clearly show, that cholesterol esters and cholesterol, although non crystallized, can co-localize in the plaque areas investigated here. It is not clear why these structures can cause SHG signals. However, the SHG sensitivity to plaque deposits that contain cholesterol derivatives is obvious.

The comparison between plaque areas which exhibited CARS and SHG signals, with areas that showed CARS but no SHG signals, using Raman microscopy clearly showed the difference in sensitivity with respect to deposits composed of triglycerides. Here, the amorphous structure of the fatty droplets does not produce SHG. Instead, because of the strong scattering cross sections of the aliphatic side chains of the triglycerides, fatty deposits can be easily detected by CARS. An interesting side observation is that although the rabbits were exposed to a heavily enriched cholesterol diet, triglycerides apparently also contributed to the plaque formations.

It was possible to collect three-dimensional image stacks with penetration depths of about 100 μm into the plaques, for the experimental conditions described here, employing approximately 60 mW, which are considered to be physiologically feasible. The focal plane of TPF and SHG signal are intrinsically the same because both signals get simultaneously excited by the 830 nm beam. Apparently, the SHG signals revealed almost exclusively the cholesterol/cholesterol ester rich plaque formations and not the underlying tissue matrix. A possible reason for that observation could be due to the epi-detection geometry that only allows detecting backward-emitted SHG light. Although in thick samples the signal can be enhanced by the back-scattered forward-emitted SHG, this is probably not enough to provide a reasonable signal level. However, why it was not possible to detect SHG signals from collagen fibrils, is not entirely clear, since Ko *et al.* did observe strong SHG signals from collagen fibrils.[13] In comparison to their findings, the deposits investigated here, were more predominant. Thus, one possibility is that the signals are overlaid by the strong SHG signals from cholesterol/cholesterol esters. Furthermore, the group detected the lipid deposits exclusively by CARS, which indicates that the deposits were mainly composed of triglycerides.

At the moment, from the cardiologists' point of view, it is particularly important to distinguish

vulnerable from stable plaque deposits. Because common medication primarily treats risk factors, such as blood pressure and circulating lipids altogether, differentiating between triglycerides and cholesterol/cholesterol esters is not of key interest in regard to systemic treatment. However, given the development of potential local treatments, as for instance coated balloon or stent dilatation, subclassification of the lipid content may become very important.

It is important not only to detect an existing plaque, but also to characterize the biochemical composition. Two aspects may be addressed in applications in humans. First of all, the possibility to distinguish vulnerable plaques from stable plaques in order to estimate the risk associated with the plaque formation. Secondly, a more personalized medication may be possible. Today patients are prescribed a combination of up to a dozen drugs, which often cause side effects. For a better characterization of the plaque compositions, the very specific spectral information obtained by Raman spectroscopy is of great advantage compared with the nonlinear techniques.

In conclusion, multimodal nonlinear imaging can represent a powerful label-free adjunct to standard histopathological methods for the analysis of arterial tissue. As demonstrated in this work, a combination of various nonlinear imaging modalities such as CARS, TPF and SHG has the potential to highlight various tissue features simultaneously, providing an optimal morphological correlation with common routine histology. Nonlinear imaging offers the strong advantage of a better resolution and contrast with respect to H&E labeling. In addition, different imaging techniques are able to selectively image various tissue components such as the connective tissue in the arterial wall and plaque deposition, with a potentially higher depth penetration than demonstrated here. In particular, SHG microscopy was found to be selective in imaging both crystalline cholesterol and cholesterol esters without crystalline structure within the deposition. The reason why the SHG signals are generated from cholesterol esters is theoretically not fully understood. The main observation from the correlation with the Raman experiments is that cholesterol esters do give rise to SHG signals, whereas triglycerides, chemically also ester compounds do not.

The capability to image the arterial wall through the plaque deposition using an *en face* geometry was demonstrated as well. On the behalf of this result and considering the recent advancements for the realization of a nonlinear optical endoscope,[26] we believe that this approach could be used *in vivo* in the near future.

Disclosure/Conflict of Interest

The authors declare no conflict of interest.

Acknowledgments

Financial support from the European Union via the Europäischer Fonds für Regionale Entwicklung (EFRE) and the "Thüringer Ministerium für Bildung Wissenschaft und Kultur (TMBWK)" (Projects: B714-07037, B578-06001, 14.90 HWP) and via the European network of excellence P4L (Photonics4Life) as well as financial support by the German Ministry for Science and Education (BMBF) *MediCARS* (FKZ: 13N10774) is highly acknowledged.

References

1. M. Naghavi, P. Libby, E. Falk, S. Casscells, S. Litovsky, J. Rumberger, J. Badimon, C. Stefanadis, P. Moreno, G. Pasterkamp, Z. Fayad, P. Stone, S. Waxman, P. Raggi, M. Madjid, A. Zarrabi, A. Burke, C. Yuan, P. Fitzgerald, D. Siscovick, C. de Korte, M. Aikawa, K. Airaksinen, G. Assmann, C. Becker, J. Chesebro, A. Farb, Z. Galis, C. Jackson, I. Jang, W. Koenig, R. Lodder, K. March, J. Demirovic, M. Navab, S. Priori, M. Rekhter, R. Bahr, S. Grundy, R. Mehran, A. Colombo, E. Boerwinkle, C. Ballantyne, W. Insull, R. Schwartz, R. Vogel, P. Serruys, G. Hansson, D. Faxon, S. Kaul, H. Drexler, P. Greenland, J. Muller, R. Virmani, P. Ridker, D. Zipes, P. K. Shah, J. Willerson, "From vulnerable plaque to vulnerable patient — A call for new definitions and risk assessment strategies: Parts I & II," *Circulation* **108**, 1664–1778 (2003).
2. D. Steinberg, A. Gotto, "Preventing coronary artery disease by lowering cholesterol levels: Fifty years from bench to bedside," *J. Med. Assoc.* **282**, 2043–2050 (1999).
3. C. Glass, J. Witztum, "Atherosclerosis; The road ahead," *Cell* **8**, 1257–1262 (2001).
4. P. Libby, M. Aikawa, "Stabilization of atherosclerotic plaques: New mechanisms and clinical targets," *Nat. Med.* **8**, 1257–1262 (2002).

5. C. M. Matter, M. Stuber, M. Nahrendorf, "Imaging of the unstable plaque: How far have we got?" *Eur. Heart J.* **30**, 2566–2575 (2009).
6. J. Huisman, M. Hartmann, C. von Birgelen, "Ultrasound and light: Friend or foe? On the role of intravascular ultrasound in the era of optical coherence tomography," *Int. J. Cardiovasc. Imaging* **27**, 209–214 (2011).
7. T. Le, H. Duren, M. Slipchenko, C. Hu, J. Cheng, "Label-free quantitative analysis of lipid metabolism in living Caenorhabditis elegans," *J. Lipid Res.* **51**, 672–677 (2010).
8. H. Rinia, K. Burger, M. Bonn, M. Müller, "Quantitative label-free imaging of lipid composition and packing of individual cellular lipid droplets using multiplex CARS microscopy," *Biophys. J.* **95**, 4908–4914 (2008).
9. R. Lim, A. Kratzer, N. Barry, S. Miyazaki-Anzai, M. Miyazaki, W. Mantulin, M. Levi, E. Potma, B. Tromberg, "Multimodal CARS microscopy determination of the impact of diet on macrophage infiltration and lipid accumulation on plaque formation in ApoE-deficient mice," *J. Lipid Res.* **51**, 1729–1737 (2010).
10. H. Wang, Y. Fu, T. Huff, T. Le, H. Wang, J. Cheng, "Chasing lipids in health and diseases by coherent anti-Stokes Raman scattering microscopy," *Vib. Spectrosc.* **50**, 160–167 (2009).
11. M. Sowa, L. Mostaco-Guidolin, M. Smith, E. Kohlenberg, A. Ridsdale, A. Stolow, A. Ko, "Nonlinear optical measurements of the artery wall: Parameters related to the progression of atherosclerosis," *Meas. Sci. Rev.* **9**, 93–94 (2009).
12. H. Wang, I. Langohr, M. Sturek, J. Cheng, "Imaging and quantitative analysis of atherosclerotic lesions by CARS-based multimodal nonlinear optical microscopy," *Arterioscler. Thromb. Vasc. Biol.* **29**, 1342–1348 (2009).
13. A. Ko, A. Ridsdale, M. Smith, L. Mostaço-Guidolin, M. Hewko, A. Pegoraro, E. Kohlenberg, B. Schattka, M. Shiomi, A. Stolow, M. Sowa, "Multimodal nonlinear optical imaging of atherosclerotic plaque development in myocardial infarction-prone rabbits," *J. Biomed. Opt.* **15**, 020501 (2010).
14. R. Cicchi, C. Matthäus, T. Meyer, A. Lattermann, B. Dietzek, B. Brehm, J. Popp, F. Pavone, "Characterization of collagen and cholesterol deposition in atherosclerotic arterial tissue using nonlinear microscopy," *J. Biophotonics*, doi: 10.1002/jbio.201300055 (2013).
15. J. Suhalim, C. Chung, M. Lilledahl, R. Lim, M. Levi, B. Tromberg, E. Potma, "Characterization of cholesterol crystals in atherosclerotic plaques using stimulated Raman scattering and second-harmonic generation microscopy," *Biophys. J.* **102**, 1988–1995 (2012).
16. R. Cicchi, N. Vogler, D. Kapsokalyvas, B. Dietzek, J. Popp, F. Pavone, "From molecular structure to tissue architecture: Collagen organization probed by SHG microscopy," *J. Biophotonics* **6**, 129–142 (2012).
17. J. Motz, M. Fitzmaurice, A. Miller, S. Gandhi, A. Haka, L. Galindo, R. Dasari, J. Kramer, M. Feld, "*In vivo* Raman spectral pathology of human atherosclerosis and vulnerable plaque," *J. Biomed. Opt.* **11**, 021003 (2006).
18. O. Sćepanović, M. Fitzmaurice, A. Miller, C. Kong, Z. Volynskaya, R. Dasari, J. Kramer, M. Feld, "Multimodal spectroscopy detects features of vulnerable atherosclerotic plaque," *J. Biomed. Opt.* **16**, 011009 (2011).
19. T. Meyer, D. Akimov, N. Tarcea, S. Chatzipapadopoulos, G. Muschiolik, J. Kobow, M. Schmitt, J. Popp, "Three-dimensional molecular mapping of a multiple emulsion by means of CARS microscopy," *J. Phys. Chem. B* **112**, 1420–1426 (2008).
20. M. Müller, A. Zumbusch, "Coherent anti-Stokes Raman Scattering microscopy," *Chemphyschem* **8**, 2156–2170 (2007).
21. M. Miljković, T. Chernenko, M. Romeo, B. Bird, C. Matthäus, M. Diem, "Label-free imaging of human cells: Algorithms for image reconstruction of Raman hyperspectral datasets," *Analyst* **135**, 2002–2013 (2010).
22. M. Hedegaard, C. Matthäus, S. Hassing, C. Krafft, M. Diem, J. Popp, "Spectral unmixing and clustering algorithms for assessment of single cells by Raman microscopic imaging," *Theor. Chem. Acc.* **130**, 1249–1260 (2011).
23. C. Krafft, L. Neudert, T. Simat, R. Salzer, "Near infrared Raman spectra of human brain lipids," *Spectrochim. Acta A: Mol. Biomol. Spectrosc.* **61**, 1529–1535 (2005).
24. C. Krafft, B. Dietzek, J. Popp, "Raman and CARS microspectroscopy of cells and tissues," *Analyst* **134**, 1046–1057 (2009).
25. A. Lattermann, C. Matthäus, N. Bergner, C. Beleites, B. Romeike, C. Krafft, B. Brehm, J. Popp, "Characterization of atherosclerotic plaque depositions by Raman and FTIR imaging," *J. Biophotonics* **6**, 110–121 (2013).
26. D. Rivera, C. Brown, D. Ouzounov, I. Pavlova, D. Kobat, W. Webb, C. Xu, "Compact and flexible raster scanning multiphoton endoscope capable of imaging unstained tissue," *Proc. Natl. Acad. Sci. USA* **108**, 17598–17603 (2011).